J Inorg Organomet Polym (2015) 25:1547–1553
DOI 10.1007/s10904-015-0274-6

ORIGINAL PAPER

Influence of Kaolin on the Sintering of Glass Powder to Glass–Ceramics

Shiquan Liu[1] · Na Li[1] · Honghai Shen[1]

Received: 4 July 2015 / Accepted: 24 August 2015 / Published online: 28 August 2015

Abstract Glass powder derived from a waste water flocculate was used to prepare sintered glass–ceramics. Different amounts of kaolin as a binder were mixed with the glass powder to form green bodies. The influence of the kaolin on the sintering, crystallization of the glass powder and on the microstructure of the obtained glass–ceramics has been investigated. DTA analysis suggests that the kaolin increases the crystallization temperature of the glass-kaolin mixtures. The results also show that the kaolin benefits reducing the sintering shrinkage of the green bodies. The kaolin does not lead to the change of crystalline phases in the sintered glass–ceramics. Instead, with an appropriate addition, the kaolin can provide reactive Al_2O_3 and SiO_2 sources due to its decomposition favoring the crystal growth and improving the mechanical property of the sintered product.

Keywords Glass–ceramic · Kaolin · Sintering · Crystallization

1 Introduction

Glass–ceramics are polycrystalline materials. They have found applications in a wide range of engineering fields, such as building materials [1], corrosion-resistant coatings [2] and optical materials [3]. Glass–ceramics are prepared by controlled crystallization of parent glasses. The controlled crystallization is mainly realized via two different routes. One is heat-treatment induced bulk crystallization [4, 5], which consists of controlled nucleation and crystal growth steps [6]. The nucleation may be initiated due to phase-separation or nucleating agents in the parent glasses [7–9]. In this case, samples are first shaped by the normal glass-forming methods (such as pressing or blowing), followed by the two-step heat-treatment. The other is sintering of the parent glass powders [10, 11], whose surfaces provide nucleation sites to initiate surface crystallization. The crystallization thus starts from the particle surface and continues inwards upon heating the glass powder at crystallization temperatures. In the meantime, viscous sintering of the glass powders results in the formation of compact samples, which are termed as sintered glass–ceramics [11].

$CaO–Al_2O_3–SiO_2$ and $CaO–MgO–Al_2O_3–SiO_2$ glasses have strong tendency to surface crystallization and it was reported that the crystallization could afford glazed tiles with high abrasion resistance and gloss [12, 13]. Glass–ceramics within these two systems have been widely fabricated via the sintering route. In the sintering mode, glass particles are either packed in refractory moulds or pressed into green bodies before sintering. The sintered glass–ceramics prepared via the crystallization of the simply packed glass particles often contain pores inside. In contrast, using the pressed green bodies could produce pore-free sintered glass–ceramics. In order to improve workability of the green bodies made from glass powders, binders have to be added [14]. Different binders, such as polyvinyl alcohol (PVA) [11], water glass ([15] and clay [16] are often used. Among them, clay is easily available and cheap [17–20]. In addition, Furlani et al. [17] has shown that chamotte from thermal treated clay enlarged sintering interval temperature of ceramic bodies and reinforced silicate glass–ceramics

✉ Shiquan Liu
liusq_ujn@hotmail.com

[1] School of Materials Science and Engineering, University of Jinan, No. 336, West Road of Nan Xinzhuang, Jinan 250022, Shandong, People's Republic of China

from wastes. To reduce the influence of impurities (such as iron and titanium compounds [17]) in clays on the color of sintered glass–ceramics, kaolin which is the main material used in white porcelains could be the best candidate as a binder in green bodies for sintering glass–ceramics [21, 22]. However, unlike an organic binder, clay minerals will undergo structural and composition changes upon heating and the components introduced by the clay binders will become a part of the final products, consequently, influence the structure and properties of the final glass–ceramics [23–25]. Therefore, effects of kaolin on the sintering and crystallization of glass powder could be complex.

Waste water flocculate used herein is a solid waste disposed by a catalyst manufacturer. At the moment, it is shipped away from the factory and buried in waste lands. However, its threat to environment of sites where it is buried is greatly concerned [16, 26]. In our previous publication, we have verified this waste into glasses with properties compatible with normal window and bottle glasses and pointed out the possibility to generate glass–ceramics using the waste as a main raw material [27]. Glass–ceramics prepared from the solid waste can be used as building materials [1]. Therefore, the production of glass–ceramics using the waste water flocculate can consume large quantities of the waste, benefiting environmental protection and resource saving [28].

In this work, kaolin was used as a binder in the green bodies of sintered glass–ceramics. The aim of this work is to investigate the influence of the added kaolin on the sintering, crystallization of the glass powder and the microstructure, properties of the sintered glass–ceramics. The study may help industrial production of sintered glass–ceramics with the waste water flocculate.

2 Materials and Methods

The kaolin was taken from the Tieshan Kaolin Refining Factory (Longyan, China). The parent glass powder used in this study was prepared using a waste water flocculate from a petroleum catalyst manufacturer as the main raw material. Details about the waste water flocculate and the glass frit preparation can be found in Ref [27].

Chemical compositions of the kaolin and the parent glass used in the study were analyzed on an S8 TIGER X-ray fluorescence (XRF) spectrometer (Bruker AXS, Germany) using fused disks prepared following the general instrument guidelines. The compositions are listed in Table 1. La_2O_3 in the glass was originated from the waste water flocculate, in which catalytic component leached into the waste water during the catalyst production. Trace elements were also present in the kaolin and determined by the XRF analysis. They are not specified here due to their low contents. Loss on ignition (LOI) of the kaolin was determined by heating the sample in a furnace at 900 °C for 2 h.

Both the kaolin and the glass particles were ground to pass a sieve of 200 mesh (particles smaller than 75 microns). They were then thoroughly mixed to produce blends, in which weight percentage of the kaolin was 0, 2, 4, 8, 10, 15 %. Accordingly, the mixtures and resultant green bodies were encoded as K0 (equal to pure glass powder sample), K2, K4, K8, K10, K15, respectively. For example, the green body K4 was made of 96 wt% glass powder and 4 wt% kaolin. To increase strength of the green bodies, an extra of 5wt% water was sprayed into each blended powder before the following shaping process [26]. Cylindrical green bodies sized Ø14.5 × 5 mm were uniaxially pressed at 75 MPa in a steel mould. The green compacts were first air-dried for 2 h and further dried in an oven at 120 °C for 2 h. Based on DTA result of the glass powder (see later in the discussion section), the green bodies were heated in a furnace with 5 °C/min to 700 °C (correspondent to the transition temperature of the glass powder), and then 3 °C/min to 850 °C. The slower heating rate at the latter stage could make easier the sintering and crystallization process. The samples were soaked at 850 °C for 30 min and cooled down to room temperature in the furnace. Designation of the sintered samples was the same as that of the green bodies.

Densification occurred during the sintering process, leading to shrinkage of the green bodies. The resultant sintering shrinkage was determined based on the difference of the sizes of the sample before and after sintering by using:

$$shrinkage\,(\%) = (L_0 - L_s)/L_0$$

where L_0, L_s are diameters of the green bodies and the corresponding sintered glass–ceramic samples [29]. In each case, three samples were measured and the values were averaged.

Crystalline phases in materials were identified by a D8 ADVANCE X-ray diffractometer (XRD) (Bruker, Germany) using Cu Kα radiation with a scanning speed of 6^{o} min^{-1}. Thermal analysis (DTA and TGA) was carried out on a differential scanning calorimeter (Hengjiu, China) with a heating rate of 5 °C/min. Microstructure of the sintered glass–ceramic was investigated on a Quanta FEG 250 scanning electron microscope (FEI, USA). Samples were first polished, and then etched in HF solution (1 %) for 30 s before the SEM examination.

Vickers hardness of the specimens was measured on an HV-10B (Huayin, China) hardness tester using indentation method. A load of 1500 mg and a loading time of 15 s were applied. For each sample, 10 different indentation tests were performed. And the data were averaged. Density

Table 1 Compositions of the parent glass powder and the kaolin used in the study (wt%)

Oxide	SiO_2	Al_2O_3	Fe_2O_3	CaO	MgO	SO_3	K_2O	Na_2O	CaF_2	La_2O_3
Parent glass	44.28	13.76	0.33	25.13	5.83	3.39	0.10	4.73	1.21	1.24
Kaolin	50.11	34.94	0.35	0.17	0.28	0.04	2.07	0.07	Trace	LOI
									0.07	11.9

of the sintered samples was measured by the method of Archimedes, according to the China National Standard (GB/T 25995-2010). The density value was obtained using the following formula:

$$\rho_a = m_1/(m_1 - m_2) \times \rho_1$$

where ρ_a, ρ_1 are the apparent density of the sintered sample and the density of distilled water, m_1 and m_2 are the dry weight and buoyant weight. Density values presented in the article were obtained on three parallel samples.

3 Results and Discussion

3.1 Analysis of the Kaolin, the Parent Glass and Their Mixtures

Figure 1 shows the DTA curve of the parent glass. The transition and crystallization temperatures of the glass are 700 and 850 °C, respectively. The sintering procedure of the green bodies was set based on this DTA result.

The XRD pattern of the raw kaolin (Fig. 2a) indicates that its main crystalline phases are kaolinite ($Al_2Si_2O_5(OH)_4$, PDF card:74-1784), quartz (SiO_2, PDF card:83-0539) and muscovite ($KAl_2Si_3AlO_{10}(OH)_2$, PDF card:86-1385). These phases remain intact when the kaolin was calcined at 510 °C (Fig. 2b). However, peak intensity of the kaolinite becomes weak. When the calcination temperature was increased to 580 °C, the diffraction peaks related to the quartz and the muscovite phases are still seen (Fig. 2c). In contrast, the peaks ascribed to the kaolinite mostly disappear. This indicates the formation of metakaolin, which has a disordered structure [30], via the following reaction [24]:

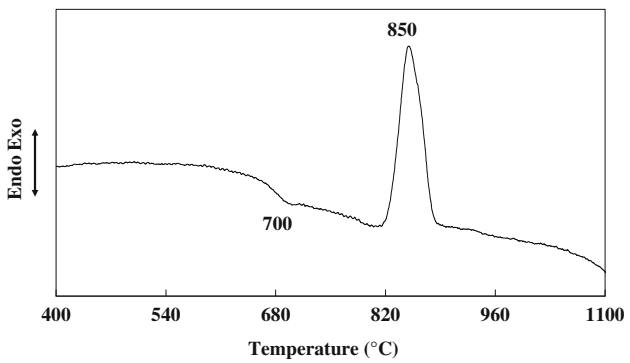

Fig. 1 DTA curve of the parent glass powder

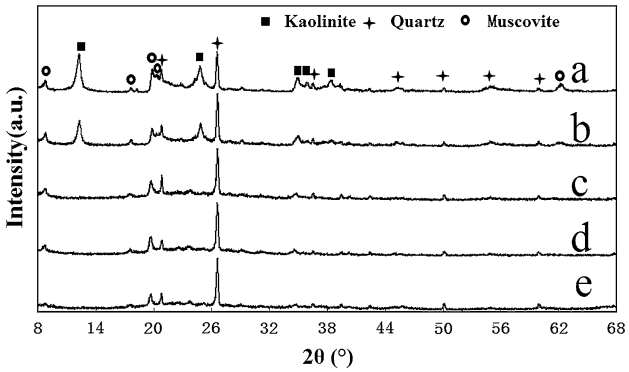

Fig. 2 XRD patterns of the raw kaolin (*a*) and the products calcined at 510 °C (*b*); 580 °C (*c*); 850 °C (*d*); 1000 °C (*e*)

$$Al_2O_3 \cdot 2SiO_2 \cdot 2H_2O \rightarrow Al_2O_3 \cdot 2SiO_2 + 2\,H_2O.$$

After further increasing the calcination temperature to 850 °C (Fig. 2d), no significant changes in the diffraction peaks are observed, because the quartz and muscovite phases are inert [25]. At 1000 °C, the amorphous metakaolin should have transformed to Al–Si spinel [24]. However, it is also amorphous and no peaks representing this phase are recognized in the XRD pattern (Fig. 2e). Finally, it should be mentioned here that the peak intensity of the muscovite is much lower than that of the quartz.

DTA-TG curves of the raw kaolin are shown in Fig. 3. The DTA curve shows two endothermic peaks at 275 and 530 °C, respectively. These two peaks are related to the removal of adsorbed water and structural water. A sharp exothermic peak is observed at 1000 °C, ascribed to the formation of Al–Si spinel. A weight loss of about 10.1 % is shown in the TG curve over the temperature range of

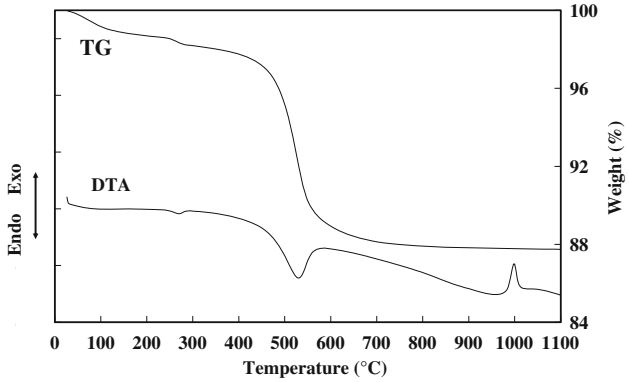

Fig. 3 DTA-TG curves of the raw kaolin

350–800 °C. This weight loss is due to the dehydroxylation of the kaolinite [24]. Based on the percentage of K_2O indicated for the kaolin in Table 1 and the above weight loss, proportions of the kaolinite, muscovite and quartz phases in the kaolin were about 72, 18 and 10 %, respectively. These mineral phases would give a mixture with the following composition: SiO_2 = 51.63 %; Al_2O_3 = 35.38 %; K_2O = 2.13 %; LOI = 10.86 %. These percentages are very close to the values given in Table 1.

DTA analysis was also performed on the glass-kaolin powder mixtures. The results are depicted in Fig. 4. The DTA curves of the glass and the kaolin are also included for comparison. It can be seen that DTA curves of the mixtures exhibit several differences in endothermic and exothermic peaks compared with those of the glass and the kaolin. From K4 to K15, the endothermic peak formerly ascribed to the removal of structural water in the kaolin becomes more visible (inset in Fig. 4, see the arrow pointing peak). In the meantime, the endothermic peak indicating the glass transition point (inset in Fig. 4, see the circled area) gradually disappears with the increase in the kaolin. We noticed that the position of the glass transition point does not change at all. Therefore, the above two differences in the DTA curves of the mixtures compared with either of its component are mainly due to mutual dilution effect upon mixing the two components. One significant change in the DTA curves is the shift of the glass crystallization peak as the dash line labeled from 850 °C of the pure glass to 900 °C of the mixture K15. The more the mixture contains kaolin, the higher the glass crystallization temperature is. In addition, the crystallization peak becomes asymmetric. This change suggests a delayed glass crystallization process of the mixtures compared with the pure glass. Moreover, the exothermic peak formerly ascribed to the formation of amorphous spinel in the kaolin (see Fig. 3) fully disappears, irrespective of the amounts of the kaolin added. The above two distinct changes above the glass transition point indicate that diffusion of the amorphous metakaolin into the glass phase occurred at a temperature before the transformation of metakaolin into spinel. This reason can also be used to explain the delayed glass crystallization process with the increase in the kaolin, because metakaolin provides the mixtures with amorphous alumina and silica (see the later discussion) [24], both of which lead to the increase in glass viscosity [31].

3.2 Influence of the Kaolin on the Sintering and Crystallization of the Glass Powder

For an easy comparison and also for the sake of energy-saving, the green bodies pressed with the mixtures containing different amounts of kaolin were all sintered at 850 °C. The sintering shrinkages of the green bodies are compared in Fig. 5. From this figure, it can be seen that the green bodies made of the pure glass and the kaolin show the largest and the smallest sintering shrinkages, respectively. The large shrinkage of K0 (the pure glass pressed sample) is due to densification of the glass powder via viscous flow sintering mechanism [32]. However, the green body of the kaolin actually was not fully densified. Open pores were detected by N_2-soprtion measurement (result not shown) [33]. The comparison also shows that the shrinkage decreases from sample K2 to K15, demonstrating that the addition of kaolin results in reduction in the sintering shrinkage of the green bodies. Quartz phase derived from the added kaolin exists in the sintered bodies (see the later XRD results) [25], contributing to reducing the sintering shrinkages [34]. This is important to protect the sintered products from deformation caused by viscous sintering of the glass [35].

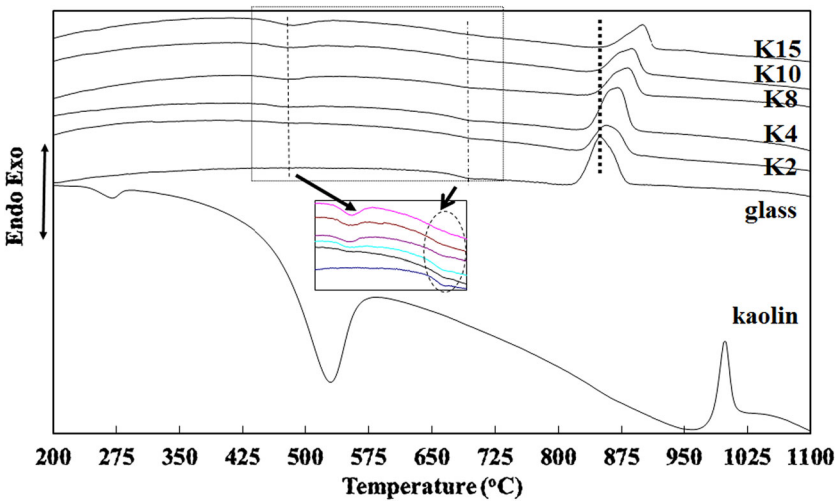

Fig. 4 DTA curves of the mixtures of the glass powder and different amounts of kaolin

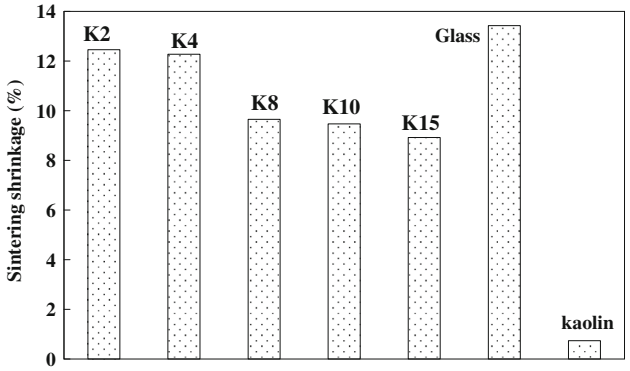

Fig. 5 Sintering shrinkages of the green bodies

The XRD patterns of the samples sintered at 580 °C and 850 °C are shown in Fig. 6a and b, respectively. Broad diffraction halos in Fig. 6a suggest that the mixtures are not crystallized upon being heated at 580 °C. Only the crystalline phases which were formerly identified in the kaolin calcined at the same temperature (see Fig. 2c) appear in the patterns of the calcined mixtures. However, due to the small amounts of the kaolin and the dilution effect of the glass powder, the diffraction peaks of the quartz, muscovite and kaolinite phases are very weak. This result also suggests that below the glass transition point, the phase transformation of the kaolin is not influenced by the mixed glass powder. In contrast, Fig. 6b indicates that all the samples calcined at 850 °C are well crystallized. In addition, intensity of the main peak slightly increases from K0 to K4, and then decreases again for K10 and K15. Irrespective of the kaolin contents, main crystalline phases in all products are identified as gehlenite (PDF card 87-0969), whose chemical formula is $Ca_2Al_2SiO_7$. A small proportion of anorthite ($CaAl_2Si_2O_8$) (PDF card 41-1486) also exists in these samples. In addition, the strongest diffraction peak ($2\theta = 26.6$) of the quartz phase is still visible in the patterns of the glass–ceramic sample K2 to sample K15 [25]. However, the muscovite phase is not revealed in the patterns of the final products due to its aforementioned lower peak intensity compared with the quartz phase [25]. Based on these XRD results, it can be concluded that the added kaolin does not change the main crystalline phases in the sintered products.

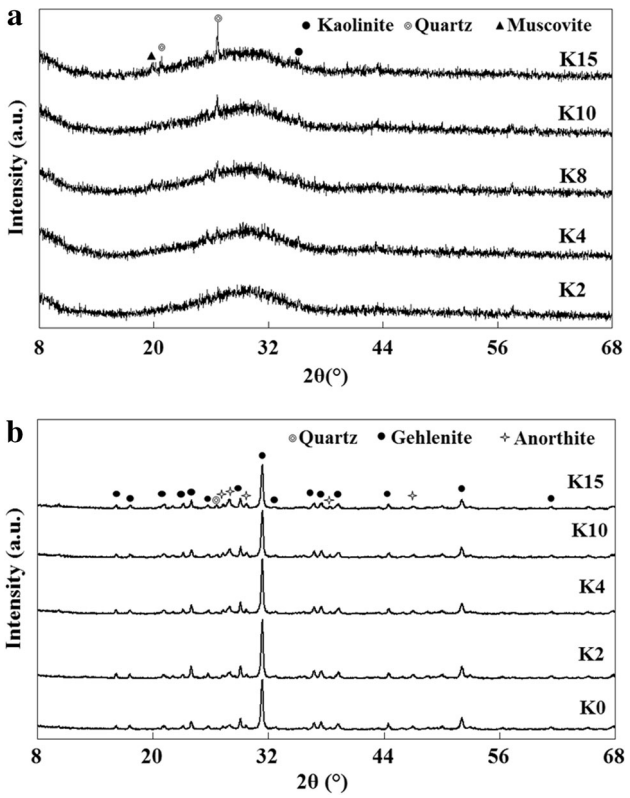

Fig. 6 XRD patterns of the samples sintered at **a** 580 °C and **b** 850 °C

The SEM images of the sintered glass–ceramic samples are shown in Fig. 7. The image of the sintered kaolin sample is also included for comparison. In the sintered kaolin sample, sheet-, sphere- and rod-like particles with different sizes coexist (Fig. 7a). The glass–ceramic samples have sphere-like crystallites distributed in a glass matrix (Fig. 7b–g). Sample K0 (Fig. 7a) (prepared without the addition of kaolin) contains mainly sphere-like crystallites, however, its microstructure is not uniform and the sphericity of the crystallites is not good. Compared with K0, samples K2 to K15 generally have larger nanocrystallites with a higher sphericity (Fig. 7c–g). It should be bear in mind that the sintering temperature (850 °C) set in the experiments is actually the best crystallization temperature for the pure glass. However, this temperature is lower than the crystallization peak temperatures of the kaolin-containing samples (see the discussion on Fig. 4 in Sect. 3.1). Therefore, the addition of kaolin favors growth of the crystallites. This can be explained as the follows. Metakaolin formed by the decomposition of kaolinite in the kaolin provides the glass mixtures with reactive sources of amorphous SiO_2 and Al_2O_3 [24]. The extra Al_2O_3 facilitates the growth of gehlenite in the glass particles upon heat treatment, because gehlenite has higher Al_2O_3/CaO and Al_2O_3/SiO_2 ratios than the parent glass (The stoichiometric composition of gehlenite is CaO 43.1 %, Al_2O_3 39.2 % and SiO_2 17.7 %. In contrast, the components in the parent glass are CaO 25.12 %, Al_2O_3 13.7 % and SiO_2 44.28 %).

From sample K0 to K2 and K4, more crystallites are formed. This is in agreement with the XRD results, in which K2 and K4 have stronger diffraction peaks than K0. K4 shows the highest crystallization among the kaolin-containing samples. Although sphericity of the crystallites in sample K8 is further well developed, residual glass phase becomes more obvious [17]. In addition, as can seen

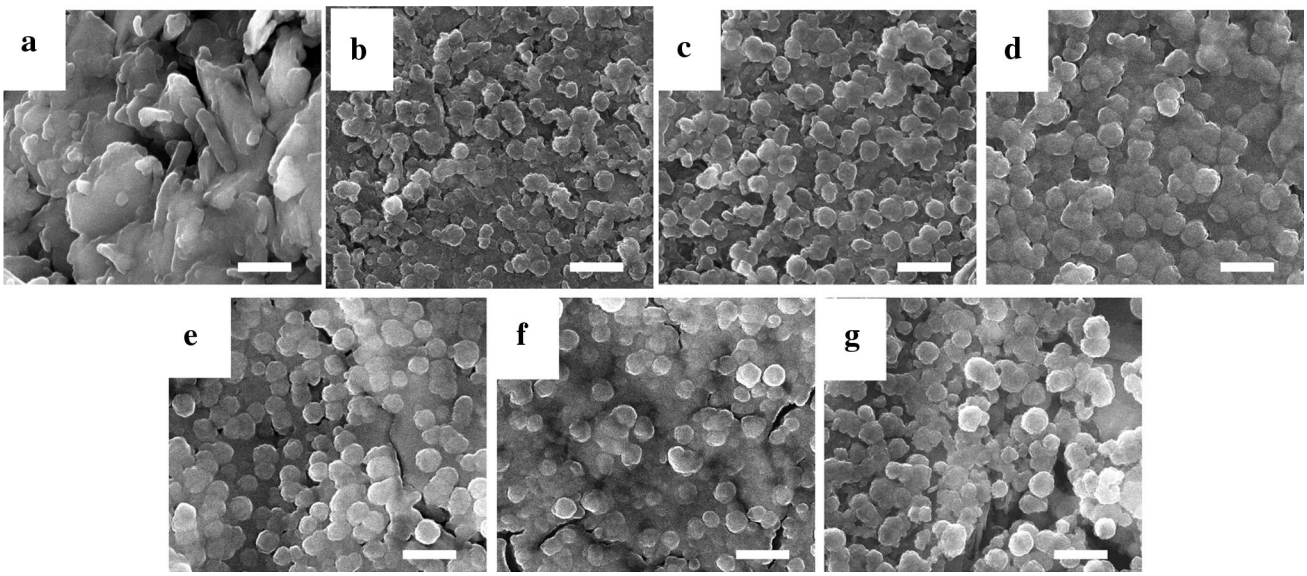

Fig. 7 SEM micrographs of the sintered kaolin (**a**), glass (**b**) and glass–ceramics K2 (**c**), K4 (**d**), K8 (**e**), K10 (**f**) and K15 (**g**)

Table 2 Density and hardness of the glass–ceramic samples

Sample	K0	K2	K4	K8	K10	K15
Density (g/cm^3)	2.72	2.69	2.75	2.68	2.66	2.62
Hardness (MPa)	3499	3475	3578	3345	3301	3210

from Fig. 7e to f, cracks appear and have an increasing trend. The cracks were generated during the cooling down process due to the thermal stress existed between the crystallites and the residual glass phase [36]. Also, the sphericity of the crystallites in sample K15 decreases (Fig. 7g). Therefore, the crystal growth is retarded when the kaolin is more than 4 %, because too much amorphous SiO_2 and Al_2O_3 provided by the metakaolin increase the viscosity of the glass phase.

Listed in Table 2 are the density and Vickers hardness values of the sintered samples. The data show that both the density and Vickers hardness first increase and then become to decrease with the increase of the kaolin. Sample K4 exhibits the highest density and hardness among all the samples studied. This is due to its more uniform crystallites, less glass phase and lack of the cracks (see Fig. 7). Therefore, the optimal amount of kaolin as the binder in the green bodies used in the study is 4 wt%.

4 Conclusions

Different amounts of kaolin were added as a binder in the green bodies for preparing sintered glass–ceramics. The results indicate that the shrinkage of the green bodies decreases and the glass crystallization temperature increases with kaolin. Compared with the sample prepared with pure glass, the glass–ceramics with the inclusion of the kaolin generally have larger nano-crystallites with a higher sphericity, suggesting that kaolin favors crystal growth. This is ascribed to the reactive amorphous SiO_2 and Al_2O_3 in metakaolin formed by the decomposition of kaolinite. In addition, kaolin does not result in change of the crystalline phases in the sintered glass–ceramics. However, too much kaolin increases the viscosity of the glass phase, leaving more residual glass un-crystallized and leading to the formation of cracks in the glass–ceramics.

Acknowledgments This work was partially supported by National Key Scientific Instruments and Equipment Development Special Fund (2011YQ140145).

References

1. T. Toya, A. Nakamura, Y. Kameshima, A. Nakajima, K. Okada, Ceram. Int. **33**, 573 (2007)
2. S. Das, S. Datta, D. Basu, G.C. Das, Ceram. Int. **34**, 1215 (2008)
3. H.N. Golshan, B.E. Yekta, V.K. Marghussian, Opt. Mater. **34**, 596 (2012)
4. C. Fredericc, E.D. Zanotto, E.C. Ziemath, J. Non-Cryst. Solids **273**, 64 (2000)
5. H. Xiao, Y. Cheng, L. Yu, H. Liu, Mater. Sci. Eng. A **431**, 191 (2006)
6. A. Hu, M. Li, D. Mao, Mater. Charact. **60**, 1529 (2009)
7. S. Golezardi, V.K. Marghussian, A. Beitollahi, S.M. Mirkazemi, J. Eur. Ceram. Soc. **30**, 1453 (2010)
8. G.A. Khater, Ceram. Int. **37**, 2193 (2011)
9. D.P. Mukherjee, S.K. Das, Ceram. Int. **39**, 571 (2013)
10. M. Rezvani, B.E. Yekta, V.K. Marghussian, J. Eur. Ceram. Soc. **25**, 1525 (2005)

11. E. Bernardo, E. Bonomo, A. Dattoli, Ceram. Int. **36**, 1675 (2010)
12. F. He, Y. Fang, J. Xie, Mater. Des. **42**, 198 (2012)
13. J.J. Reinosa, F. Rubio-Marcos, E. Solera, J.F. Fernández, Ceram. Int. **36**, 1845 (2010)
14. http://digitalfire.com/4sight/education/binders_for_ceramic_bodies_345.html
15. W. Liang, Y. Tu, H. Zhou, C. Liu, C. Rüssel, J. Non-Cryst. Solids **357**, 958 (2011)
16. E. Bernardo, R.D. Maschio, Waste Manag. **31**, 2245 (2011)
17. E. Furlani, G. Tonello, S. Maschio, E. Aneggi, D. Minichelli, S. Bruckner, E. Lucchini, Ceram. Int. **37**, 1293 (2011)
18. H.H. Murray, Appl. Clay Sci. **17**, 207 (2000)
19. I. Rozenstrauha, D. Bajare, R. Cimdins, L. Berzina, J. Bossert, A.R. Boccaccini, Ceram. Int. **32**, 115 (2006)
20. M.R. Sahar, K. Hamzah, M.S. Rohani, K.A. Samah, M.M. Razi, Phys. Proc. **22**, 125 (2011)
21. I. Ponsot, R. Falcone, E. Bernardo, Ceram. Int. **39**, 6907 (2013)
22. W. Zhang, H. Gao, Y. Xu, J. Eur. Ceram. Soc. **31**, 1669 (2011)
23. L. He, Study on the Calcination of Washed-kaolin and the Properties of Products, South China University of Technology, China (2011)
24. J. Malaiskiene, R. Maciulaitis, A. Kicaite, Constr. Build. Mater. **25**, 3168 (2011)
25. R. Alonso-Santurde, A. Coz, J.R. Viguri, A. Andrés, Constr. Build. Mater. **27**, 97 (2012)
26. O. Kizinievic, R. Zurauskiene, V. Kizinievic, R. Zurauskas, Constr. Build. Mater. **41**, 464 (2013)
27. N. Li, Y. Tuo, H. Shen, S. Liu, Ceram. Int. **39**, 8667 (2013)
28. R.D. Rawlings, J.P. Wu, A.R. Boccaccini, J. Mater. Sci. **41**, 733 (2006)
29. N.Y. Mostafa, A.A. Shaltout, M.S. Abdel-Aal, A. El-maghraby, Mater. Des. **31**, 3677 (2010)
30. E. Gámiz, M. Melgosa, M. Sánchez-Marañón, J.M. Martín-García, R. Delgado, Appl. Clay Sci. **28**, 269 (2005)
31. H. Scholze (translated by M.J. Lakin), Glass, Nature, Structure and Properties. (Spring, New York, 1990)
32. M.J. Pascual, A. Durán, L. Pascual, J. Non-Cryst. Solids **306**, 58 (2002)
33. V. Mymrine, M.J.J.S. Ponte, H.A. Ponte, N.M.S. Kaminari, U. Pawlowsky, G.J.P. Solyon, Constr. Build. Mater. **41**, 360 (2013)
34. M. Eberstein, S. Reinsch, R. Müller, J. Deubener, W.A. Schiller, J. Eur. Ceram. Soc. **29**, 2469 (2009)
35. E. Verné, R. Defilippi, G. Carl, C.V. Brovarone, P. Appendino, J. Eur. Ceram. Soc. **23**, 675 (2003)
36. E. Bernardo, G. Scarinci, Ceram. Int. **30**, 785 (2004)